

Effect of spin diffusion on spin torque in magnetic nanopillars

Sergei Urazhdin and Scott Button

Department of Physics, West Virginia University, Morgantown, WV 26506

We present systematic magnetoelectronic measurements of magnetic nanopillars with different structures of polarizing magnetic layers. The magnetic reversal at small magnetic field, the onset of magnetic dynamics at larger field, and the magnetoresistance exhibit a significant dependence on the type of the polarizing layer. We performed detailed quantitative modeling showing that the differences can be explained by the effects of spin-dependent electron diffusion.

PACS numbers: 72.25.Ba, 72.25.RB, 75.47.De

According to the spin torque (ST) model¹, current-induced magnetic switching (CIMS) in magnetic multilayers is caused by angular momentum transfer from the conduction electrons to the magnetic layers. ST is believed to occur within atomic distances from the magnetic interfaces. Nevertheless, theories have shown that electron diffusion in the layers has an important effect on ST.^{2,3,4} As a simple example, an electron scattering between two ferromagnets transfers angular momentum upon each reflection. However, this transfer is not necessarily associated with a net charge current I . Therefore, efficient utilization of electron scattering can result in reduced I required to manipulate magnetic devices with ST. In a more subtle manifestation, spin-dependent electron diffusion causes an asymmetry between the ST in antiparallel (AP) and parallel (P) configurations of the magnetic layers.⁵ In an extreme case of such asymmetry, ST can change direction, resulting in anomalous current-induced behaviors.⁶

Despite extensive theoretical work, few experiments addressed the effects of diffusion on ST.^{6,7,8,9,10} The main difficulty stems from the limited knowledge about the transport properties of individual layers in magnetic nanostructures. Different deposition and measurement techniques yielded significantly different values.¹¹ On the other hand, both the Magnetoresistance (MR) and CIMS depend on the same spin-dependent transport properties. Therefore, simultaneous measurements of MR and CIMS, and their analysis within the same theoretical framework can lead to better understanding of the electron diffusion and its effect on ST.

We report systematic measurements of MR and CIMS in nanopillar spin valves $F_1/N/F_2$ with identical free layers $F_2=\text{Py}(5)$, $\text{Py}=\text{Ni}_{80}\text{Fe}_{20}$, and different polarizers F_1 incorporating Co. Thicknesses are given in nm. Large spin diffusion length $l_{sf,Co}$ makes Co ideal for studying the effects of diffusion. We used $F_1=\text{Co}(20)$ in samples labeled $Co20$. To separate the contributions of the Co interfaces and its bulk, we tested samples with $F_1=\text{Co}(3)$, labeled $Co3$, in which the scattering in the bulk of $\text{Co}(3)$ was negligible. To eliminate the spin diffusion in the sample contacts, we inserted a strongly spin flipping bilayer $\text{Fe}_{50}\text{Mn}_{50}(1)/\text{Cu}(1)$ between $\text{Co}(3)$ and the bottom contact in samples labeled $FeMnCo3$.

The multilayers $\text{Cu}(50)/F_1/\text{Cu}(10)/F_2/\text{Cu}(200)$ were

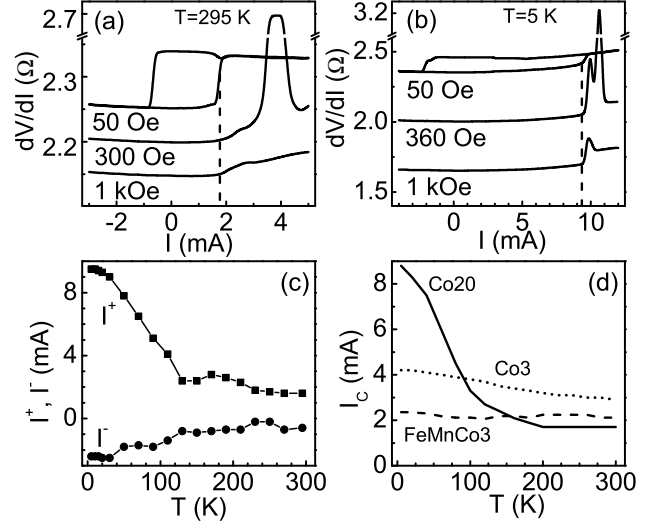


FIG. 1: (a) dV/dI vs I at labeled H and $T = 295$ K. Curves are offset for clarity. (b) same as (a), at $T = 5$ K. (c) I^+ , I^- vs T for a $Co20$ sample. (d) I_c vs T measured at $H = 500$ Oe for the three types of samples as labeled.

deposited at room temperature 295 K (RT) by magnetron sputtering at base pressure of 5×10^{-9} Torr, in 5 mTorr of purified Ar. F_2 and part of the $\text{Cu}(10)$ spacer were patterned into an elliptical nanopillar with approximate dimensions 130×60 nm. We measured dV/dI with four-probes and lock-in detection. Positive I flowed from F_1 to F_2 . Magnetic field H was in the film plane and along the nanopillar easy axis. At least three nanopillars of each type were tested with similar results.

Figs. 1(a),(b) show dV/dI vs I for a $Co20$ sample, acquired at RT and 5 K, respectively. The data at small $H = 50$ Oe are characterized by hysteretic jumps to the P state with low resistance R_P at $I^- < 0$, and to the AP state with high resistance R_{AP} at $I^+ > 0$. At $H = 300/360$ Oe in Figs. 1(a)/(b), the jumps are replaced by large peaks caused by the reversible transition between the P and AP states.¹² The onset of the magnetic dynamics starting at $I = I_c$ appears as a sharp increase of dV/dI nearly independent of H (1 kOe data in Figs. 1(a),(b)). The approximate equality $I_c \approx I^+$ shown with a dashed line indicates that the reversal oc-

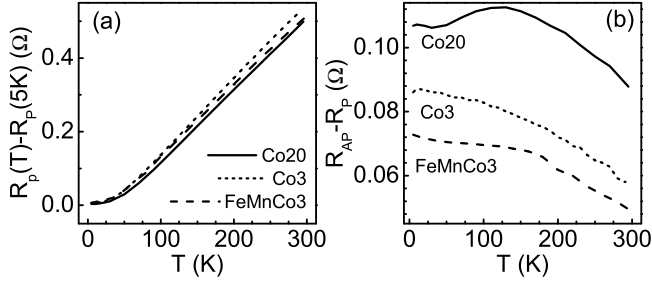


FIG. 2: (a) P-state resistances R_P offset by values at 5 K, and (b) MR *vs* T for the three types of samples as labeled.

curs when large-amplitude dynamics is excited by ST. The 5 K data exhibit significantly increased reversal currents and I_C . Fig. 1(c) summarizes the temperature dependence of I^+ and I^- . Both are nearly constant above 130 K, below which they dramatically increase. Similar behaviors of Co/Cu/Co nanopillars indicate their intrinsic origin from the spin-dependent transport in Co.⁸

One may attribute some of the dependence on T shown in Fig. 1(c) to the effects of thermal activation. Indeed, $I^+ \leq I_C$ at RT because thermal fluctuations result in reversal slightly before the onset of large-amplitude dynamics. In contrast, $I^+ \geq I_C$ at 5 K because current-induced dynamics can occur before the reversal occurs. The fundamental quantity predicted by the models of ST is I_C . It is insensitive to thermal fluctuations and sample shape imperfections, and can be directly determined from the sharp increase of dV/dI at H large enough to suppress hysteretic reversal. Fig. 1(d) summarizes I_C *vs* T for all three different sample structures. *FeMnCo3* data are approximately independent of T , while I_C for *Co3* and *Co20* increase when T is decreased. Comparing panels (c) and (d) reveals that I_C closely follows I^+ . It is not possible to measure a similar excitation onset current I_C^- in the AP state, because transition to the P state is not suppressed at any H . Below, we use I^- as an approximation for I_C^- .

Since F_2 is identical in all samples, the different behaviors of I_C must be attributed to the different spin-dependent transport properties of F_1 . The difference between *Co3* and *FeMnCo3* is due to the spin flipping in FeMn, which eliminates spin diffusion in the bottom Cu(50) contact. The difference between the *Co20* and *Co3* data indicates that the effects of spin diffusion in Co are stronger than those in Cu. Despite a significant increase of I_C in *Co20*, it does not diverge as would be expected if the sign of ST was reversed.⁶

Figs. 2(a),(b) show temperature dependence of $R_P - R_P(0)$ and MR = $R_{AP} - R_P$. R_P increased with T due to magnon and phonon scattering, and were surprisingly consistent among the samples. Interestingly, there is a clear correlation between the variations of MR and I_C in all samples. As T decreases from RT, all MRs increase at a similar rate, while I_C slightly increase. At lower T , the trends for *Co3* and *FeMnCo3* remain the same, while

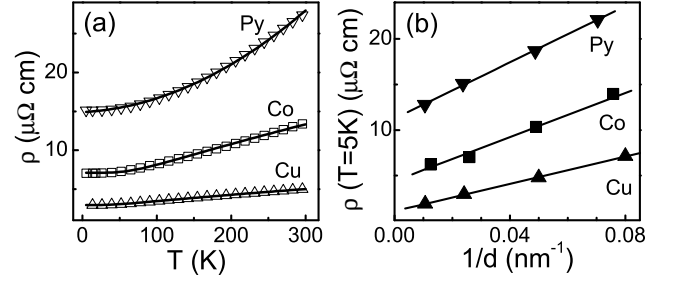


FIG. 3: (a) Resistivities of 40 nm thick Py, Co, and Cu films measured in Van der Pauw geometry. The Co and Cu data are fitted with the Bloch-Gruneisen approximation, with Debye temperatures $\theta_{Co} = 373$ K and $\theta_{Cu} = 265$ K. The Py data are fitted with a quadratic dependence. (b) Dependencies of residual resistivities on inverse film thickness (symbols), with linear fits shown.

a decrease of MR in *Co20* at $T < 130$ coincides with a sharp increase of I_C .

To understand the dependencies of MR, CIMS, and I_C on the sample structure, we performed simultaneous calculations of spin-dependent transport and ST. Our model combines a diffusive approximation for the ferromagnets and outer sample contacts with a ballistic approximation for the Cu(10) spacer between the ferromagnets.⁵ This approximation is consistent with calculations based on the Boltzmann equation.¹⁴ We combine the continuity conditions for spin currents and spin accumulation in the spacer between F_1 and F_2 derived by Slonczewski⁵ (Eqs. (13),(14)) with a small-angle expansion of Eq. (28) for ST. The resulting expression for ST in terms of the spin current $I_s = I^\uparrow - I^\downarrow$ and spin accumulation $\Delta\mu = \mu^\uparrow - \mu^\downarrow$ in the Cu(10) spacer near the collinear magnetic configuration is

$$\tau = \frac{\hbar \sin(\theta)}{4e} (AG\Delta\mu - I_s) \quad (1)$$

where e is the electron charge, \hbar is the Planck's constant, G is twice the mixing conductance introduced in the circuit theory,² A is the area of the nanopillar, and θ is the angle between the magnetic moments. At $I = I_C$, τ compensates the damping torque, yielding

$$I_C = \frac{\alpha e \gamma S_2 2\pi M_2}{\tau}, \quad (2)$$

where $\alpha \approx 0.03$ is the Gilbert damping parameter,¹⁵ γ is the gyromagnetic ratio, τ is ST determined from Equation (1) at $I = 1$ in appropriate units, and $S_2 = M_2 V / 2\mu_B$ is the total spin of the Py(5) nanopillar. Here, V is the volume of F_2 , and μ_B is the Bohr magneton. The magnetization M_2 of Py varied from 730 emu/cm^3 at 20 K to 675 emu/cm^3 at 300 K, as determined by magnetometry of Py(5) films prepared under the same conditions as the nanopillars. These values are lower than expected for bulk Py, but consistent with the published results for Py films.¹⁶

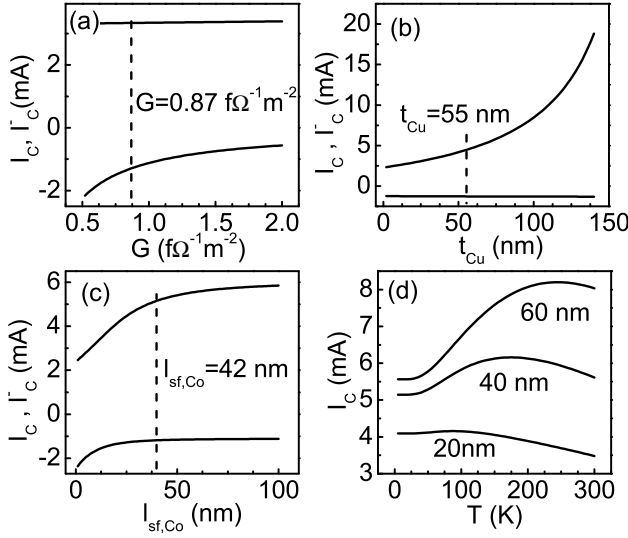


FIG. 4: (a) Calculated I_C, I_C^- vs G for $FeMnCo3$. (b) Same vs t_{Cu} for $Co3$. (c) Same vs $l_{sf,Co}$ for $Co20$, (d) same vs T for $Co20$ samples, for the residual values of $l_{sf,Co}$ as labeled.

Equations (1) and (2) express I_C in terms of $\Delta\mu$ and I_S , the same quantities that determine MR in magnetic multilayers. We calculated $\Delta\mu$ and I_S self-consistently using a one-dimensional diffusive approximation employing the standard MR parameters: spin asymmetries β , renormalized resistivities $\rho^* = \rho/(1 - \beta^2)$, spin diffusion lengths l_{sf} in the layers, and similarly defined parameters AR^* , γ , and δ for the interfaces.¹⁷ We estimate these parameters from a combination of the published values¹¹ and our own measurements, as described below.

The resistivity of each layer in our samples provides essential information about electron diffusion. Because of variations among published resistivities, we instead determined their values from measurements of thin films prepared under the same conditions as the nanopillars, with thicknesses verified by x-ray reflectometry. Fig. 3(a) shows $\rho(T)$ for 40 nm thick Py, Co, and Cu films, together with fittings for Co and Cu with the Bloch-Grüneisen approximation. We obtained better fitting for Py data with a quadratic dependence, indicating that electron-magnon scattering may dominate electron-phonon scattering.¹⁸ The dependence of the residual resistivity on film thickness was consistent with the Fuchs-Sommerfeld approximation (Fig. 3(b)), allowing us to extract the bulk residual values $\rho_{Py}(0) = 11.3 \mu\Omega\text{cm}$, $\rho_{Co}(0) = 4.4 \mu\Omega\text{cm}$, and $\rho_{Cu}(0) = 1.1 \mu\Omega\text{cm}$. We used the extracted bulk $\rho(T)$ to model all the extended layers in the nanopillars. The effect of lateral confinement in Py(5) nanopillars was approximated by using the resistivity of a Py(40) film.

To estimate $l_{sf}(T)$, we used its empirical inverse relationship with ρ , along with the bulk residual values $l_{sf,Py}(0) = 6$ nm, and $l_{sf,Cu}(0) = 300$ nm based on published measurements,¹¹ scaled by the somewhat different residual resistivities of our films. If scattering by thermal excitations does not flip electron spins, a weaker depen-

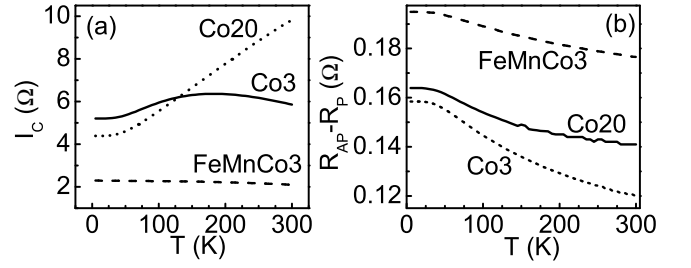


FIG. 5: (a) Calculated I_C vs T , and (b) calculated MR vs T for three sample types as labeled.

dence $l_{sf}(T) \propto \sqrt{1/\rho(T)}$ is possible. However, we show below that a dependence even stronger than $1/\rho$ is more likely. We use $\beta_{Py} = \gamma_{Py/Cu} = 0.7$, $\gamma_{Co/Cu} = 0.8$, $\beta_{Co} = 0.36$ for spin asymmetries, $AR_{Co/Cu}^* = 0.55 f\Omega m^2$, $AR_{Py/Cu}^* = 0.5 f\Omega m^2$ for renormalized interface resistances, and $\delta_{Co/Cu} = 0.2$, $\delta_{Py/Cu} = 0.25$ for spin flipping coefficients.^{8,11} Their dependence on T is neglected due to the dominance of the band structure and impurity scattering far from the Curie temperature. For FeMn, we used $l_{sf,FeMn} \approx 0.5$ nm, and $\rho_{FeMn} = 87 \mu\Omega\text{cm}$. Scattering at its interfaces was modeled by adding 0.5 nm to the nominal thickness of FeMn. To account for the Cu contacts, the calculation included outer Cu layers of thickness t_{Cu} , determined as described below. These layers were terminated with fictitious spin sinks.

To demonstrate that CIMS is extremely sensitive to the effects of diffusion, we now describe how our 5 K data can be fitted by appropriate choice of three parameters whose values have the largest uncertainty: conductance G in Equation (1), effective MR-active thickness t_{Cu} of the Cu contacts, and spin diffusion length $l_{sf,Co}$. Calculations for $FeMnCo3$ were significantly affected only by G , which controls the asymmetry of CIMS. The values of $I_C/|I^-|$ in mA measured at 5 K for three $FeMnCo3$ samples were 2.3/0.8, 1.6/0.6, and 3.1/1.5, giving an average ratio $I_C/|I^-| = 2.6$. The calculated value increases from 1.46 at $G = 0.5 f\Omega^{-1}m^{-2}$ to 6.1 at $G = 2 f\Omega^{-1}m^{-2}$ (Fig. 4(a)). The best values $I_C/|I^-| = 3.34/1.27$ are obtained at $G = 0.87 f\Omega^{-1}m^{-2}$, in reasonable agreement with band structure calculations.^{5,19}

Spin diffusion in the bottom Cu layer has little effect on $Co20$ and $FeMnCo$ due to the spin relaxation in Co and FeMn, respectively. To determine t_{Cu} , we use the ratios $I_C/|I^-|$ of the three $Co3$ samples, 3.55/1.0, 4.6/1.5, and 4.2/1.2, giving an average ratio $I_C/|I^-| = 3.4$. The calculated $I_C/|I^-|$ increases from 1.9 for $t_{Cu} = 0$ to 14 for $t_{Cu} = 140$ nm (Fig. 4(b)), and eventually diverges at $t_{Cu} = 200$ nm. The best agreement with data is obtained for $t_{Cu} = 55$ nm, resulting in $I_C/|I^-| = 4.4/1.3$.

Lastly, diffusion in Co significantly affects CIMS in samples $Co20$, but not in $Co3$ and $FeMnCo3$. We determine $l_{sf,Co}$ from the ratio $I_C/|I^-|$ of five $Co20$ samples, 8.9/2.1, 7.3/1.6, 9.0/2.0, 8.5/2.0, 8.0/1.7, giving an average ratio $I_C/|I^-| = 4.4$. Fig. 4(c) illustrates that the

calculated ratio $I_C/|I_C^-|$ increases from 1.0 for $l_{sf,Co} = 0$ to 5.2 for $l_{sf,Co} = 100$ nm. The best agreement with the data is obtained for $l_{sf,Co} = 42$ nm consistent with the published values.¹¹

Despite the ability to model the 5 K data, the calculations did not reproduce the dramatic dependence of I_C on T in Fig. 2 (see below). Therefore, one can attempt to determine $l_{sf,Co}$ from the dependence of I_C on T . Fig. 4(d) shows calculations for the residual values $l_{sf,Co} = 20$ nm, 40 nm, and 60 nm. Large $l_{sf,Co}$ results in I_C decreasing with T , which is inconsistent with the data. Small $l_{sf,Co}$ gives decrease of I_C with T in better qualitative agreement with data, but gives unreasonably small I_C at 5 K. Consequently, we return to the value determined from Fig. 4(c).

Fig. 5(a) shows the calculated I_C vs T for the three sample types. To interpret these results, we note that Figs. 4(b)-(d) exhibited an increase of I_C when the effective MR-active resistance of F_1 determined by ρl_{sf} was increased. This relationship was also established analytically.^{5,20} The experimental correlation between the decreases of MR and increases of I_C in Figs. 1, 2 is of the same origin. The lack of temperature dependence for *FeMnCo3* is therefore consistent with negligible spin diffusion effects in F_1 . In calculations for *Co3*, the increase of I_C with T is caused by the increased contribution $t_{Cu}l_{sf,Cu}$ to the effective resistance of F_1 . Calculations for *Co20* show a competition between the contribution of the bulk Co resistivity, which increases with T , and the contributions from the Cu(50) layer and the outer Co/Cu interface, which decrease with T due to the increased spin flipping in Co. However, both *Co3* and *Co20* calculations do not reproduce the data, suggesting that the effects of thermal scattering should be re-examined.

The calculated dependence of MR on T was in over-

all agreement with data for *Co3* and *FeMnCo3*, but did not reproduce the decrease at $T < 130$ K seen in *Co20* data (Fig. 5(b)). The calculations overestimated the values, suggesting that our samples may be larger than their nominal size. However, this seems to contradict the calculated temperature dependence of R_P consistent with the data (not shown), and the values of I_C that are larger than the measured 5 K values. This discrepancy can be reduced e.g. by decreasing $l_{sf,Py}$, which results in a decreased MR without significantly affecting CIMS.

The failure of *Co20* calculations to capture the decrease of MR and the increase of I_C at $T < 130$ K indicates that $l_{sf,Co}$ decreases with T more rapidly than the accepted $l_{sf} \propto 1/\rho$, resulting in the reduction of the effective MR-active resistance $\rho_{Co}l_{sf,Co}$. One possible mechanism for such a strong dependence may be electron-magnon scattering which can result in electron spin flipping without significant momentum scattering. We leave more detailed and perhaps alternative explanations to future studies.

To summarize, we performed magnetoelectronic measurements of nanopillars with three different polarizing magnetic layers. The samples exhibited different current-induced behaviors, attributed to the spin diffusion in the polarizing layer. The calculations reproduced the lower temperature behaviors with reasonable values of transport parameters. However, temperature dependencies of magnetoresistance and current-induced switching indicate that the effects of thermal scattering on spin transport are more significant than presently believed.

We thank Mark Stiles, Jack Bass and Norman Birge for helpful discussions. This work was supported by NSF Grant DMR-0747609 and a Research Corporation Cottrell Scholar Award. SB acknowledges support from the NASA Space Grant Consortium.

-
- ¹ J. Slonczewski, J. Magn. Magn. Mater. **159**, L1 (1996).
 - ² A.A. Kovalev, A. Brataas, and G.E.W. Bauer, Phys. Rev. **B 66**, 224424 (2002).
 - ³ S. Zhang, P.M. Levy, and A. Fert, Phys. Rev. Lett. **88**, 236601 (2002).
 - ⁴ A. Shpiro, P.M. Levy, and S. Zhang, Phys. Rev. **B 67**, 104430 (2003).
 - ⁵ J. Slonczewski, J. Magn. Magn. Mater. **247**, 324 (2002).
 - ⁶ O. Boulle, V. Cros, J. Grollier, L.G. Pereira, C. Deranlot, F. Petroff, G. Faini, J. Barnas, and A. Fert, Nature Physics **3**, 492 (2007).
 - ⁷ S. Urazhdin, N.O. Birge, W.P. Pratt Jr., and J. Bass, Appl. Phys. Lett. **84**, 1516 (2004).
 - ⁸ T. Yang, A. Hirohata, M. Hara, T. Kimura, and Y. Otani, Appl. Phys. Lett. **89**, 252505 (2006).
 - ⁹ M. AlHajDarwish, H. Kurt, S. Urazhdin, A. Fert, R. Loloee, W. P. Pratt, Jr., and J. Bass, Phys. Rev. Lett. **93**, 157203 (2004).
 - ¹⁰ N. Theodoropoulou, A. Sharma, W.P. Pratt Jr., and J. Bass, Phys. Rev. **B 76**, 220408(R) (2007).
 - ¹¹ J. Bass and W.P. Pratt Jr., JMMM **200**, 274 (1999) and J. Phys.: Condens. Matter **19**, 183201 (2007).
 - ¹² S. Urazhdin, N.O. Birge, W.P. Pratt Jr., and J. Bass, Phys. Rev. Lett. **91**, 146803 (2003).
 - ¹³ S.D. Steenwyk, S.Y. Hsu, R. Loloee, J. Bass, and W.P. Pratt Jr., J. Magn. Magn. Mater. **170**, L1 (1997).
 - ¹⁴ J. Xiao, A. Zangwill, and M.D. Stiles, Phys. Rev **B 70**, 172405 (2004).
 - ¹⁵ I.N. Krivorotov, N.C. Emley, J.C. Sankey, S.I. Kiselev, D.C. Ralph, and R.A. Buhrman, Science **307**, 228 (2005).
 - ¹⁶ I.N. Krivorotov, N.C. Emley, A.G.F. Garcia, J.C. Sankey, S.I. Kiselev, D.C. Ralph, and R.A. Buhrman, Phys. Rev. Lett. **93**, 166603 (2004).
 - ¹⁷ T. Valet and A. Fert Phys. Rev. **B 48**, 7099 (1993).
 - ¹⁸ D.A. Goodings, Phys. Rev. **132**, 542 (1963).
 - ¹⁹ K. Xia, P.J. Kelly, G.E.W. Bauer, A. Brataas, and I. Turek, Phys. Rev. **B 65**, 220401R (2002).
 - ²⁰ S. Urazhdin, R. Loloee, and W. P. Pratt Jr., Phys. Rev. **B 71**, 100401 (2005).
 - ²¹ J. Bass and W.P. Pratt Jr., private communications.